Biophysical Journal, Volume *110*

Supplemental Information

Cholesterol Increases the Openness of SNARE-Mediated Flickering Fusion Pores

Benjamin S. Stratton, Jason M. Warner, Zhenyong Wu, Joerg Nikolaus, George Wei, Emma Wagnon, David Baddeley, Erdem Karatekin, and Ben O'Shaughnessy

Biophysical Journal

Supporting Material

Cholesterol Increases the Openness of SNARE-Mediated Flickering Fusion Pores

Benjamin S. Stratton,[1] Jason M. Warner ,[1] Zhenyong Wu,[2,3] Joerg Nikolaus,[2,3] George Wei,[1] Emma Wagnon,[1] David Baddeley,[3,4] Erdem Karatekin,[2,3,5,6,*] and Ben O'Shaughnessy[1,*]

[1]Department of Chemical Engineering, Columbia University, New York, New York; [2]Department of Cellular and Molecular Physiology, Yale University, School of Medicine, New Haven, Connecticut; [3]Nanobiology Institute, Yale University, West Haven, Connecticut; [4]Department of Cell Biology and [5]Department of Molecular Biophysics and Biochemistry, Yale University, New Haven, Connecticut; and [6]Laboratoire de Neurophotonique, Université Paris Descartes, Centre National de la Recherche Scientifique (CNRS) UMR8250, Paris, France

*Correspondence: bo8@columbia.edu; erdem.karatekin@yale.edu

Decomposition of the docking-to-fusion delay time distribution into a fast and a slow component

For each fusion event, following docking of a vesicle onto the SBL fusion occurred after a delay time τ_{delay} (Fig. **2**B, C). We measured τ_{delay} from the TIRF signal and for each lipid composition we constructed the distribution of delay times, represented as the survivor function $S(\tau_{\mathrm{delay}})$, the probability fusion has not occurred after a time τ_{delay} (Fig. **S2**E). From these distributions we found that there are two populations of fusion events: a fast-fusing population and a slowly fusing population with significantly longer delay times, similarly to ref. (1). Following ref. (1) we interpreted the fast fusers as being SNARE-dependent, and the slow fusers as originating in non-specific events and involving fusion pores whose dynamics were not controlled by SNAREpins. This enabled us to measure the effects of SNARE proteins on flickering fusion pore dynamics, and to study by comparison the dynamics of fusion pores that are apparently controlled only by the lipid membranes independently of SNAREs, consistent with ref. (1).

The survivor distributions were well fit by mixed exponentials of the form $S(\tau_{\mathrm{delay}}) = a\exp(-\tau_{\mathrm{delay}}/\overline{\tau}_{\mathrm{delay}}) + (1-a)\exp(-\tau_{\mathrm{delay}}/\overline{\tau}_{\mathrm{ns}})$ where a is the amplitude of the fast fusing component and is interpreted as the fraction of vesicles which fuse in a SNARE-mediated manner, $\overline{\tau}_{\mathrm{delay}}$ is the mean docking-to-fusion delay time for SNARE-mediated fusion, and $\overline{\tau}_{\mathrm{ns}}$ is the mean delay time for non-specific fusion. Fits were obtained using a maximum likelihood estimate using Matlab's Statistics Toolbox. $\overline{\tau}_{\mathrm{ns}}$ was in the range $\sim 2-3$ s for all compositions, ~10 times greater than typical mean delay times for specific SNARE-mediated events.

Method to identify events as fast or slow. We determined a maximum cutoff time for the specific SNARE-mediated events, and defined all events with τ_{delay} less (greater) than this time to be specific (non-specific) events. The cutoff time was determined as follows. As the parameter a represents the fraction of fusion events which are SNARE-mediated, we varied the cutoff time until the fraction of fusion events below this cutoff time matched a from the double exponential fit. For self-consistency, we checked that the cutoff time was larger than the mean value of the delay time for the fast fusers and smaller than the mean value of the delay time for the slow

fusers. The cutoff times we find, ~70-600 ms (Fig. **S2**E), are ~2-6-fold greater than $\overline{\tau}_{\mathrm{delay}}$ and ~4-fold smaller than $\overline{\tau}_{\mathrm{ns}}$.

The statistics of fusion events between v-SUVs and protein-free SBLs are similar to those for the slow component of fusion events between v-SUVs and t-SBLs. We also examined fusion events between protein-free SBLs (pf-SBLs) and v-SNARE containing SUVs (v-SUVs). To test that the slow component of the fusion events between t-SNARE containing SBLs (t-SBLs) and v-SUVs represented events for which the fusion pore dynamics were SNARE-independent, we compared $\overline{\tau}_{\mathrm{ns}}$ to $\overline{\tau}_{\mathrm{pf}}$, the mean value of the delay time for pf-SBL/v-SUV fusion events. For membranes with 45% (10%) cholesterol in the SUV (SBL) we found $\overline{\tau}_{\mathrm{pf}} \sim 1.9$ s, statistically indistinguishable from $\overline{\tau}_{\mathrm{ns}}$ for the same composition, Fig. 5A ($p>0.05$). Similarly, for the same composition the openness $P_0 \sim 0.05 \pm 0.02$ of pf-SBL/v-SUVs fusion pores was statistically indistinguishable from the pore openness for the slow component of the t-SBL/v-SUV fusion events ($P>0.05$, see non-specific events in Fig. 4C).

These observations are consistent with the hypothesis that the fusion pore dynamics of the slow component of t-SBL/v-SUV events are determined by the physical properties of the lipid bilayers.

Properties of single fluorescent lipids in the SBL

In the main text (*SNARE-mediated fusion pores flicker or are permanently open*, in Results) we fit the predicted total intensity time course, eq. 3, to the measured integrated intensity time course $I_{\mathrm{tot}}(t)$ for each fusion event to determine the pore openness and vesicle size (Fig. 4). In order to perform this fit, we required three single lipid properties: the single fluorescent lipid intensity I_{lip} in the SBL, the fluorescent lipid bleaching time in the SBL τ_{bleach}, and the single lipid diffusivity D_{lip} (Fig. **S2**). Almost all fluorescent spots released into the SBL upon fusion remained bright for a period and then suddenly darkened (bleached) in a single frame, consistent with these spots being single fluorescent lipids. In this way, for each lipid we made a 'digital' measurement of the bleaching time. We confined our single lipid analysis to those which

bleached in one step in this manner. Fluorescent lipids were tracked using SpeckleTrackerJ (2), and further analysis was performed using Matlab.

Measurement of single fluorescent lipid intensity, $I_{\mathbf{lip}}$. We measured the intensity of a single lipid by measuring the average change of intensity upon bleaching. We take the average of the total intensity of a lipid in an area $3x3$ pixels ($0.80\ x\ 0.80\ \mu m^2$) centered on the lipid, time-averaged over the final 15 frames for which the lipid fluoresced. We measured the background intensity in the same location where the lipid bleached, over the 15 frames following bleaching. The latter was subtracted from the former to determine the intensity of the individual lipid. We then averaged each of these individual lipid intensities over ~40 lipids to determine the mean single lipid intensity I_{lip} for a given movie, ~1 min in duration (i.e. Fig. **S2**A). All analysis of events from that movie used the measured single lipid intensity from that movie.

Measurement of single lipid diffusion coefficient, $D_{\mathbf{lip}}$. We calculated the mean square displacement (MSD) for lipid trajectories lasting $\gtrsim$ 1.5 seconds and determined the best fit linear relation of MSD vs. t over time windows ranging from one to 10 frames ($t_{\mathrm{frame}} \approx$ 17 ms or 31 ms) to sample a full range of the trajectory. A sample of 7 of these MSD curves is shown in Fig. **S2**B. We then calculated the diffusion constant from $\mathrm{MSD} = MSD(0) + 4\,D_{\mathrm{lip}}\,t$ for each analyzed trajectory. We report a mean $\pm$ SEM D_{lip} averaged from ~20 analyzed lipid trajectories for each lipid composition, Table **S3**. The MSD was calculated in Matlab.

Measurement of lipid bleaching time in the SBL, $\tau_{\mathbf{bleach}}$. We measured the lipid bleaching time τ_{bleach} by determining the total duration of single lipid trajectories and then calculating the survivor function $f_{\mathrm{fluor}}(t)$ describing many such trajectories. We fit a decaying exponential to the survivor function $f_{\mathrm{fluor}}(t) = e^{-t/\tau_{\mathrm{bleach}}}$ (Fig. **S2C**). Approximately 50 bleaching episodes were used to calculate the survivor function in each movie. The uncertainty reported is the 95% confidence interval from the fitting routine.

The bleaching rate in the vesicle is much slower than that in the SBL. Our measurements of single lipid bleaching were for lipids in the SBL. To determine bleaching rates for lipids in vesicles (expected to be lower since the fluorescence emission is lower) we measured the bleaching time of entire vesicles $\tau_{\mathrm{bleach}}^{\mathrm{ves}}$ for ~ 30 vesicles that did not fuse per movie. We measured $\tau_{\mathrm{bleach}}^{\mathrm{ves}}$ from the best fit exponential $I_{\mathrm{tot}}(t) = I_{\mathrm{o}} \exp(-t/\tau_{\mathrm{bleach}}^{\mathrm{ves}})$ (Fig. S2D). I_{tot} is

the spatially integrated intensity over a box of size 15x15 pixels centered on the unfused vesicle, with the background subtracted off. Repeating this for each movie, we found that the bleaching time in vesicles is ~5-8-fold greater than the bleaching time in the SBL. Thus, when we used our model to calculate the fluorescence intensity versus time, $I_{tot}(t)$, we neglected fluorescent bleaching of lipids in the vesicle (eqs. **3, 4**).

Analysis of individual fusion events.

For each fusion event, we measured the total intensity versus time *t*, $I_{\mathrm{tot}}(t)$ (Fig. 2B and C). To do this, we measured the integrated intensity by drawing a square region of interest of size $30x30$ pixels. We use a box of this size to ensure that all of the lipids remain in the box for the duration of the measurement, 1.6 s. We analyzed fusion events with longer release times by manually drawing larger boxes based on the specific fusion event. Fusing vesicles were well spaced enough that we did not have to account for significant background lipid diffusion into the region of interest.

In TIRFM the evolving fluorescence intensity following a SUV-SBL fusion event provides a high time resolution readout of lipid transfer. As described in the main text, when lipids diffuse from a vesicle into the SBL through the walls of a fusion pore a rapid increase in fluorescence intensity is observed due to the spatial decay of the intensity of the incident evanescent wave, and the change in mean lipid orientation when a lipid transfers to the planar SBL from the spherical SUV which alters the coupling to the polarized evanescent wave. The increase in fluorescence is instantaneous upon transfer of a labeled lipid into the SBL and thus provides a very sensitive measure of the fraction of dye transferred between the fusing membranes as a function of time, with temporal resolution limited only by acquisition frame rates (~100 Hz, which is in turn limited by the exposure time needed to detect single fluorophores). In conjunction with a mathematical model of release through a flickering pore, this enabled us to accurately measure SUV-to-SBL lipid release times τ_{release}. A fitting procedure using the mathematical model was needed because the lipid release kinetics are convoluted with bleaching kinetics (Fig. 2C).

By comparison the spread of the dye from the fusion site to a distance larger than the optical resolution (~250 nm) would take 60 ms or longer (taking D_{lip}=1 $\mu m^2 s^{-1}$), too slow to measure typical release times. In a previous work where we employed the present SUV-SBL fusion assay, but used far-field fluorescence microscopy rather than TIRFM, the signal of fusion was taken to be this spread of lipids from the fusion site, quantified by the time course of the width of a two-dimensional Gaussian profile fit to the image sequence representing a fusing vesicle (1).

A different kind of resolution limit determines the minimum flickering frequency our method can access. When a flickering pore opens (Fig. S1A), if it remains open for longer than the time for all labelled lipids to diffuse out of the vesicle through the open pore, the signal will be lost before completion of a single flicker cycle. This diffusion time is approximately τ_{ves}, the lipid diffusion time for a distance of order the vesicle size (multiplied by a logarithmic factor of order unity involving the pore diameter). Thus when we observe a pore openness <1, indicating that the release time exceeds τ_{ves}, the most we can say is that the flickering frequency is higher than this lower limit. Given τ_{ves}~ 10ms for a typical vesicle size, it follows that the pores we measure flicker at frequencies $\gtrsim 100$ Hz. A similar limitation holds for amperometry, once the contents have been released, the pore may continue to flicker without being observed.

Dependence of fusion statistics on vesicle size

Fusion pore statistics do not depend on vesicle size. Over the vesicle size range ($10\,nm \lesssim R_{ves} \lesssim 80\,nm$) and lipid compositions studied, our data did not reveal correlations between vesicle size and either docking-to-fusion delay times, pore openness P_o or the fraction of pores that were permanently open (Fig. **S4**A-C).

Fusion probability does not depend on vesicle size. A fraction of vesicles dock but do not fuse within the time the labelled lipids in the vesicle have completely bleached. Thus we sought to determine whether these vesicles followed a different size distribution to vesicles that fused, as this would suggest size-dependence in the fusion mechanism.

For these events where fusion does not occur we could not use our usual procedure to measure vesicle size, which is based on fitting our model to a fluorescence intensity versus time curve

I_{tot}(t) during a fusion event. Thus, to obtain the size distribution of such vesicles, we measured the docked vesicle intensity I_{dock} (Fig. 2**C**) and to deduce the vesicle radius R_{ves} we used the best fit power law relation $R_{\mathrm{ves}} = 2.6\left(I_{\mathrm{dock}}/I_{\mathrm{lip}}\right)^{0.61}$ obtained from the assembled data from this study (Fig. **6C**).

We then compared this distribution of non-fusers to the vesicle size distribution for vesicles that underwent SNARE-mediated fusion. The comparison showed that the size distributions were statistically indistinguishable (Fig. **S4D**).

Calculation of relation between pore openness and lipid release time

In the main text ("Fusion pore openness P_{o} is quantitatively related to lipid release time τ_{release}" in Results) we presented results to a mathematical model of diffusion of labeled lipids from the membrane of a vesicle through a flickering fusion pore into the SBL membranes, eqs. 1, 3, and 4. Here, we describe the derivation of these results, specifically the results for P_{o} as a function of vesicle area A_{ves} and lipid release time τ_{release} (eq. 1), and the time dependent TIRF intensity emission $I_{\mathrm{tot}}(t)$ for both a flickering pore and a permanently open pore (eqs. 3 and 4 of the main text).

We will show below that $\phi_{ves}(t)$ decays exponentially in time for a flickering pore. In parallel, we will show that for the special case of a fully open pore the release kinetics are instead of power law form, $\phi_{\mathrm{ves}} \sim 1/t$ (eq. 3).

The flickering pore is open for a fraction P_{o} of the time and closed for a fraction $1 - P_{\mathrm{o}}$ of the time. The starting point of the model is the time evolution of the density of labelled lipids in the vesicle, $n(\boldsymbol{x}, \boldsymbol{t})$ and in the SBL, $\rho(\boldsymbol{r}, \boldsymbol{t})$ (Fig. **S1**A).

$$\partial \mathrm{n}/\,\partial \mathrm{t} = D_{\mathrm{lip}}\nabla^2 n \;-\; Q(t)\delta(\boldsymbol{x}), \qquad \partial \rho/\,\partial \mathrm{t} = D_{\mathrm{lip}}\nabla^2 \rho \;+\; Q(t)\delta(\boldsymbol{r}), \qquad \textbf{S1}$$

where D_{lip} is the lipid diffusivity. From these fields, we calculate the fraction of labelled lipids remaining in the vesicle, $\phi_{\mathrm{ves}}(t)$. The driving force for lipid release from the vesicle into the SBL is the density difference across the fusion pore, $n_0(t) - \rho_0(t)$. The lipid release rate $Q(t)$ is the product of this density difference and the pore transmission coefficient k_{pore}

$$Q(t) = \; k_{\mathrm{pore}}\{n(0,t) - \rho(0,t)\}, \qquad d\phi_{ves}/dt \; = -Q(t)/n_0 A_{\mathrm{ves}}\,, \qquad \textbf{S2}$$

where k_{pore} is the pore transmission coefficient and n_{o} the initial density of labeled lipids in the vesicle of area A_{ves}. For simplicity, we take the pore as a cylinder of height b and radius r_{p}, commonly assumed in the interpretation of pore conductances (3-6). The release rate is then the flux through a cylindrical membrane tube of cross-sectional length $2\pi r_{\mathrm{p}}$, i.e.

$$k_{\mathrm{pore}} = P_{\mathrm{o}}\, D_{\mathrm{lip}} 2\pi \mathrm{r_p}/\mathrm{b}. \qquad \textbf{S3}$$

Note that k_{pore} is reduced by the pore openness, P_{o}, which for a two-state (open/closed) pore is the fraction of the time the flickering pore is in the open state. More generally, for a pore whose size changes continuously up to some maximum size in the fully open state, P_{o} is the mean pore radius relative to the maximum value.

We consider two cases: an infrequently open flickering pore (eq. 1) and a permanently open pore (eq. 3). We then calculate the total TIRF intensity as a function of time, $I_{\mathrm{tot}}(t)$, for each case, allowing us to extract lipid release times τ_{release}, vesicle sizes R_{ves}, and pore openness P_{o} for individual fusion events.

The solutions to eq. S1 can be written:

$$\begin{aligned} n(\boldsymbol{x},\boldsymbol{t}) &= \mathbf{n}_{\mathrm{a}} - \textstyle\int_0^t \boldsymbol{dt'}\mathbf{Q}(\mathbf{t'})\mathbf{G_s}(\mathbf{0},\mathbf{x},\mathbf{t}-\mathbf{t'}) \\ \rho(\mathbf{r},\mathbf{t}) &= \textstyle\int_0^t \boldsymbol{dt'}\mathbf{Q}(\mathbf{t'})\mathbf{G}(\mathbf{0},\mathbf{r},\mathbf{t}-\mathbf{t'}) \end{aligned}, \qquad \textbf{S4}$$

where $\mathbf{G_s}(\mathbf{x'},\mathbf{x},\mathbf{t})$ is the Green's function of the diffusion equation in the vesicle, the probability a lipid in the vesicle at $\mathbf{x'}$ diffuses to $\mathbf{x}$ a time $\mathbf{t}$ later, and $\mathbf{G}(\mathbf{r'},\mathbf{r},\mathbf{t})$ is the same for the SBL. Setting $\mathbf{r}=\mathbf{x}=0$ and including eq. S1 and S2 gives:

$$\begin{aligned} n_0(t) &= n_{\mathrm{a}} - \textstyle\int_0^t dt' g(t-t') \\ \rho_0(t) &= \textstyle\int_0^t dt' Q(t') S(t-t') \\ Q(t) &= k_{\mathrm{pore}}\left(n_0(t) - \rho_0(t)\right) \end{aligned} \qquad \textbf{S5}$$

where g and S are the return probabilities for the vesicle and the SBL respectively, namely the Green's functions evaluated at $\mathbf{x}=\mathbf{x'}$ and $\mathbf{r}=\mathbf{r'}$, respectively, and n_0, ρ_0 denote the densities at $\mathbf{x}$=0 and $\mathbf{r}$=0, respectively. In general, k_{pore} fluctuates with time. However, since measured flickering timescales are far less than the lipid release time we assumed that k_{pore} can be treated as a constant, the effective time-averaged value.

Laplace transforming $t \to E$, the solution is:

$$
\begin{aligned}
Q &= \frac{k_{\mathrm{pore}} n_{\mathrm{a}}}{E\left[1+k_{\mathrm{pore}}\left(g(E)+S(E)\right)\right]}\,, \\
\rho_0 &= \frac{k_{\mathrm{pore}} n_{\mathrm{a}} S}{E\left[1+k_{\mathrm{pore}}\left(g(E)+S(E)\right)\right]}\,, \\
n_0/n_{\mathrm{a}} &= \frac{k_{\mathrm{pore}} S}{E\left[1+k_{\mathrm{pore}}\left(g(E)+S(E)\right)\right]}\,,
\end{aligned}
\qquad \textbf{S6}
$$

where $Q(E), \rho_{\mathrm{o}}(E), n_0(E), g(E), S(E)$ are all functions of E. Note that G is a simple 2D Gaussian describing free lipid diffusion in the SBL. Thus, $S(t) = 1/4\pi D_{\mathrm{lip}}\, t$, and a crude approximation of its Laplace transform is $S(E) \approx \left(1/D_{\mathrm{lip}}\right) \ln(1/E t_{\mathrm{b}})$ where $t_{\mathrm{b}} = b^2/D_{\mathrm{lip}}$ and b is a pore cut-off scale.

Lipid release through a flickering fusion pore. If $k_{\mathrm{pore}} \ll D_{\mathrm{lip}}$, then $S(E) \ll 1/k_{\mathrm{pore}}$ for any $E > t_{\mathrm{b}}^{-1} e^{1/\epsilon}$, where $\epsilon = k_{\mathrm{pore}}/D_{\mathrm{lip}}$. Thus for small enough ϵ, for all relevant E we can delete the $k_{\mathrm{pore}}\, S$ terms in eq. S3. In addition, we can replace $g(E) \approx 1/E A_{\mathrm{ves}}$ with its form for small E ($E < 1/\tau_{\mathrm{ves}}$) reflecting the fact that on time scales greater than τ_{ves} a point source uniformly covers the vesicle. We justify this below. Thus, eq. **S5** gives:

$$
\begin{aligned}
n_0 &= \frac{n_{\mathrm{a}}}{E + k_{\mathrm{pore}}/A_{\mathrm{ves}}} \\
\rho_0 &= \frac{k_{\mathrm{pore}} n_{\mathrm{a}} S}{E + k_{\mathrm{pore}}/A_{\mathrm{ves}}} \\
Q &= k_{\mathrm{pore}} n_0
\end{aligned}
\qquad \textbf{S7}
$$

The solution is $n_0(t) = n_a \exp(-t/\tau_{\mathrm{release}})$ where $\tau_{\mathrm{release}} = A_{\mathrm{ves}}/k_{\mathrm{pore}}$. Using the expression for k_{pore} in eq. S3, we arrive at the expression for pore openness P_{o} in terms of τ_{release} and A_{ves} of eq. 1 of the main text. Using the expression for Q in eq. S7 in eq. S2 gives

$$
\phi_{\mathrm{ves}} = \exp(-t/\tau_{\mathrm{release}}) \qquad \textbf{S8}
$$

In this limit, $n(x,t) \approx n_0(t)$ is uniform because the release time greatly exceeds the vesicle diffusion time (since $\tau_{\mathrm{release}}/\tau_{\mathrm{ves}} = 1/\epsilon \gg 1$). Further, the fraction released by time τ_{ves} is thus very small. Since $g(t)$ assumes its long time form ($1/A_{\mathrm{ves}}$) for times $t > \tau_{\mathrm{ves}}$, this justifies our replacing $g(E)$ with its long time form to obtain eq. **S8**: these are the only time scales relevant to the decay of ϕ_{ves}.

TIRF intensity time course through a flickering fusion pore. In this subsection we derive the expression of eq. 2 in the main text for the time-dependent total fluorescence intensity of labelled

lipids during a fusion event. The total intensity I_{tot} is the sum of the intensity of lipids in the vesicle and the intensity of lipids released into the SBL. The calculation of this quantity rests on three principal features. (i) When a lipid in a SUV is released into the SBL its emission increases by a factor $1/\lambda_{\mathrm{TIRF}}$. (ii) We ignore lipid bleaching in SUVs, being significantly slower than for lipids in the SBL (Figs. **S3C**, **D**). (iii) When a lipid is released through a flickering pore into the SBL, in this small k_{pore} limit that defines a flickering pore it is very unlikely to diffuse back into the vesicle. This follows from the fact that $n_0 \ll \rho_0$ in this flickering pore limit, for which $\mathrm{k}_{\mathrm{pore}}\, S \ll 1$ (see eq. S7), so the current of lipids is almost completely unidirectional from SUV to SBL (see eq. 2 of main text).

The total intensity for a vesicle is the sum of the contributions of fluorescent lipids which remain in the vesicle, and those that are in the SBL and have not yet bleached. The initial number of lipids in the vesicle is $N_{\mathrm{ves}}^{\mathrm{a}} = n_{\mathrm{a}} A_{\mathrm{ves}}$. The number of lipids in the vesicle decays as eq. S8, that is $N_{\mathrm{ves}}(t) = N_{\mathrm{ves}}^{\mathrm{a}} \exp(-t/\tau_{\mathrm{release}})$. The rate of fluorescent lipid addition to the SBL is the same magnitude as the rate of lipid release from the vesicle. Thus, the number of fluorescent lipids in the SBL, $N_{\mathrm{SBL}}(t)$, obeys

$$\frac{dN_{SBL}}{dt} = \frac{N_{\mathrm{ves}}(t)}{\tau_{\mathrm{release}}} - \frac{N_{\mathrm{SBL}}(t)}{\tau_{\mathrm{bleach}}},$$

where we used the fact that for this flickering pore case spatial variations in density in the vesicle can be ignored ($n(x,t) \approx n_0(t) = N_{\mathrm{ves}}(t)/A_{\mathrm{ves}}$). The solution is

$$N_{\mathrm{SBL}}(t) = \frac{N_{\mathrm{ves}}^{\mathrm{a}}\left(e^{-t/\tau_{\mathrm{bleach}}} - e^{-t/\tau_{\mathrm{release}}}\right)}{(1 - \tau_{\mathrm{release}}/\tau_{\mathrm{bleach}})}. \qquad \textbf{S9}$$

Hence the total intensity is given by

$$I_{\mathrm{tot}}(t) = I_{\mathrm{lip}} \lambda_{\mathrm{TIRF}} N_{\mathrm{ves}}(t) + I_{\mathrm{lip}} N_{\mathrm{SBL}}(t) \qquad \textbf{S10}$$

where $N_{SBL}(t)$ is given by eq. S9 and $N_{\mathrm{ves}}(t) = N_{\mathrm{ves}}^{\mathrm{a}} \exp(-t/\tau_{\mathrm{release}})$. As the vesicle intensity at the instant of fusion is $I_{\mathrm{fus}} = I_{\mathrm{lip}} \lambda_{\mathrm{TIRF}} N_{\mathrm{ves}}^{\mathrm{a}}$, we obtain $I_{\mathrm{tot}}(t)$ in terms of τ_{release}, λ_{TIRF}, and τ_{bleach} of eq. 2 in the main text by plugging eq. **S9** and the expression for $N_{\mathrm{ves}}(t)$ above into eq. **S8**.

The case of a permanently open pore. For a fully open pore, $P_{\mathrm{o}} = 1$, eq. S3 tells us that $k_{\mathrm{pore}} = D_{\mathrm{lip}} 2\pi r_{\mathrm{p}}/b$. Thus k_{pore} is of order D_{lip} ($\epsilon \approx 1$), and $k_{\mathrm{pore}}\, S(E) \gg 1$ for all $E \gg t_{\mathrm{b}}^{-1}$, ie for all relevant E. Thus from eq. **S6**

$$\rho_o \approx n_0 \approx n_{\mathrm{a}} A_{\mathrm{ves}} S(E) \qquad \textbf{S11}$$

Consider the behavior for $E \ll 1/\tau_{\mathrm{ves}}$. On these time scales $ES < 1/A_{\mathrm{ves}}$ and we have

$$\rho_{\mathrm{o}}(E) \approx n_0(E) \approx n_{\mathrm{a}} A_{\mathrm{ves}} S(E), (E < 1/\tau_{\mathrm{ves}}) \qquad \textbf{S12}$$

Thus $n_0(t)$ decays as $S(t) = 1/(4\,\pi D_{\mathrm{lip}} t)$, and $\phi_{\mathrm{ves}}(t) \approx n_0(t)/n_{\mathrm{a}} = A_{\mathrm{ves}} S(t)$. Hence we obtain eq. 4 of the main text $\phi_{\mathrm{ves}}(t) = \tau_{\mathrm{ves}}/t$. The form of the net TIRF signal $I_{\mathrm{tot}}(t)$ is modified from eq. 3 of the main text. Unlike flickering pores, reverse diffusion is significant through an open pore: typical lipids transit the fusion pore many times and lipids which have bleached will reenter the vesicle, just as fluorescing lipids will. Thus, all lipids have equal probability of bleaching and the predicted TIRF fluorescence intensity $I_{\mathrm{tot}}(t)$ for permanently open pores is thus eq. 4 of the main text.

Calculation of the number of SNARE complexes at the fusion pore using the t-SNARE recruitment model of ref. [1]

In the main text ("At high cholesterol levels fusion is so accelerated that there is insufficient time to recruit t-SNAREs to the fusion site," Fig. **5**A) we report the number of t-SNAREs recruited during the docking-to-fusion delay time by vesicle v-SNAREs using the SNARE recruitment model that we previously developed in ref. (1). This procedure provides an estimate of the number of SNAREpins involved in fusion for each membrane composition, reported in Fig. **5**A of the main text.

t-SNARE recruitment model. In ref. (1), we developed a t-SNARE recruitment model to determine the number of t-SNAREs, $N^{\star}$, recruited to the vesicle a time τ after the vesicle is docked by formation of the first SNARE complex. The key model assumptions were: (1) t-SNAREs are homogeneously and randomly distributed throughout the SBL with density Γ_{S} and diffuse independently with diffusivity D_{S}; (2) when a t-SNARE diffuses into the "reaction sink"

region of radius b beneath the vesicle, it immediately binds an available vesicle v-SNARE to form a SNAREpin; (3) fusion occurs instantly when p SNAREpins have formed. Thus solving the reaction-diffusion equation governing t-SNARE diffusion and binding with v-SNAREs, the model-predicted mean number of t-SNAREs recruited after time τ is

$$N^{\star}(\tau) = \frac{4\pi\Gamma_{\mathrm{S}} D_{\mathrm{S}} \tau}{\ln(c_1 \tau/\tau_{\mathrm{b}})}, \tau_{\mathrm{b}} = b^2/D_{\mathrm{S}}\,, \qquad \textbf{S13}$$

where the numerical constant $c_1 = 1.247$. Here we evaluate eq. **S13** at the measured mean delay time to fusion ($\tau = \overline{\tau}_{\mathrm{delay}}$). Thus after accounting for the initial SNAREpin which docks the vesicle, the total number of SNAREpins p participating in the fusion process for that vesicle is

$$p = \frac{4\pi\Gamma_{\mathrm{S}} D_{\mathrm{S}} \overline{\tau}_{\mathrm{delay}}}{\ln(c_1 \overline{\tau}_{\mathrm{delay}}/\tau_{\mathrm{b}})} + 1 \qquad \textbf{S14}$$

Below we estimate the values of the parameters in eq. **S14** and thus estimate the number of SNAREpins recruited for each membrane composition, $p - 1$.

Parameter values. To evaluate the t-SNARE diffusivity, we assumed the ratio $D_{\mathrm{s}}/D_{\mathrm{lip}}$ remained constant across different compositions and equal to 0.10, the value of this ratio that was used in ref. (1) based on the SNARE diffusivity measured by Wagner and Tamm (7). Using the single lipid diffusivity values of Table S**3** for all SBL compositions gives t-SNARE diffusivities of 0.17, 0.12, 0.15, and 0.04 μm^2/s. Assuming that the mobile, active fraction of t-SNAREs in the SBL is 0.5 (1, 7), the density of mobile t-SNAREs is $\Gamma_{\mathrm{S}} = 41.67/\mu m^2$ for our lipid to protein ratio (t-L:P=20,000). We take the sink size b=10 nm as in ref. (1).

Recruitment model predictions. Let us define $n = p - 1$ to be the number of t-SNAREs recruited to the fusion site before fusion occurs. Using the parameter estimates above in eq. **S14** predicts $n = 6 \pm 3$ and $n = 3 \pm 1$ for the model composition and the cholesterol free physiological composition PC/PS and PC/PS/PE/PIP2, respectively, and $n = 3 \pm 2$ for physiological compositions with 45% cholesterol in the SUV membranes and 10% cholesterol in the SBL membranes. (Note the reported uncertainties in n are lower-bounds estimated by propagating only the uncertainty in τ_{delay} values.) These n values are consistent with the range n ~ 3-10 reported in refs. (1, 8). In clear contrast, the same procedure when applied to physiological compositions with 46% cholesterol in both the SUV and SBL membranes

predicted that only $n = 0.15 \pm 0.02$ SNAREpins are recruited during the delay to fusion, suggesting that there is insignificant time for even a single additional t-SNARE to be recruited to the fusion site after docking.

As discussed in the main text, this could indicate that t-SNAREs are preclustered at docking sites with high densities.

Dependence of the TIRF fluorescence reduction factor $\boldsymbol{\lambda_{\mathrm{TIRF}}}$ on vesicle radius $\boldsymbol{R_{\mathrm{ves}}}$: coupled contributions from incident evanescent intensity decay and polarization effects

In Fig. **6D** of the main text we plotted values of $\boldsymbol{\lambda_{\mathrm{TIRF}}}$ versus $\boldsymbol{R_{\mathrm{ves}}}$ obtained from our analyses of many fusion events. Here, we discuss the theoretical relationship between these two quantities based on the known characteristics of TIRF microscopy. From this relation we determined the tangent of the relation at zero vesicle radius and we fit the tangent to the data of Fig. **6D.**

Consider a vesicle of radius R_{ves} docked at the SBL as in Fig. **6**A. The total TIRF fluorescence emission intensity of the vesicle is a sum over all lipid orientations θ in the spherical vesicle membrane

$$I_{\mathrm{dock}} = \epsilon I_{\mathrm{inc}}^{\mathrm{o}} \rho_{\mathrm{lip}} \mu_{\mathrm{Q}} \int_0^{\pi} d\theta 2\pi R_{\mathrm{ves}}^2 \sin\theta \, \alpha_{\mathrm{P}}(\theta) e^{-R_{\mathrm{ves}}[1+\cos\theta]/\delta_{\mathrm{TIRF}}} . \qquad \textbf{S15}$$

Here $I_{\mathrm{inc}}^{\mathrm{o}}$ is the incident TIRF intensity at the SBL ($z = 0$), ϵ is the single fluorescent lipid emissivity, δ_{TIRF} is the TIRF decay length and $\mu_{\mathrm{Q}} \leq 1$ is the fluorescence quenching factor due to a higher labeled lipid density in the vesicle. The mean polarization factor per lipid, $\alpha_{\mathrm{P}}(\theta)$, is the factor by which the lipid intensity is reduced (or enhanced) due to its orientation, for a segment of the vesicle bilayer with outward normal oriented at angle θ relative to the SBL normal. We define this factor relative to the situation when the lipid resides in the SBL ($\theta = 0$): hence $\alpha_{\mathrm{P}}(0) \equiv 1$. It arises because the evanescent TIRF wave is polarized, and preferentially excites fluorescent labels whose excitation dipoles align with its polarization (9). α_{P} is the mean value per lipid, and is a weighted average over all labeled lipids in the inner and outer monolayers of the local vesicle segment. In general it is expected to depend on bilayer curvature,

labeled and unlabeled lipid density and the partitioning of labeled lipids between the two monolayers.

Following fusion of the vesicle, the labeled lipids will be released into the SBL and after sufficient time will have diffused to be dilute enough for full dequenching to have occurred. The polarization factor for the lipids is then unity. Thus, the total intensity of the released lipids in the SBL is given by:

$$I_{\mathrm{dock}} = \epsilon I^{\mathrm{o}}_{\mathrm{inc}} \rho_{\mathrm{lip}} 4\pi R^2_{\mathrm{ves}} \qquad \textbf{S16}$$

The fluorescence reduction factor is the ratio of the total intensities before and after fusion:

$$\lambda_{\mathrm{TIRF}}(R_{\mathrm{ves}}) = \frac{I_{\mathrm{dock}}}{I_{\mathrm{SBL}}} = \frac{\mu_{\mathrm{Q}}}{2} \int_0^{\pi} d\theta \sin\theta \, \alpha_{\mathrm{P}}(\theta) e^{-R_{\mathrm{ves}}[1+\cos\theta]/\delta_{\mathrm{TIRF}}} \qquad \textbf{S17}$$

We are interested in the form of λ_{TIRF} as a function of R_{ves}. It is clear from the integral in eq. **S17** that this dependence is complex, as the effects of exponential TIRF intensity fall off and polarization are intimately coupled. Both effects are important. The only practical way to establish this crucial function, $\lambda_{\mathrm{TIRF}}(R_{\mathrm{ves}})$, is to directly measure it as described in the main text (Fig. **6**D).

Determining the pure polarization effect. Now taking the derivative of $\lambda_{\mathrm{TIRF}}(R_{\mathrm{ves}})$ with respect to R_{ves} and setting $R_{\mathrm{ves}} = 0$, one obtains a sum of two terms, $-\lambda_{\mathrm{TIRF}}(0)/\delta_{\mathrm{TIRF}} + \left(\mu_{\mathrm{Q}}/2\right) \int_0^{\pi} d\theta \sin\theta \cos\theta \, \alpha_{\mathrm{P}}(\theta)$. The second term vanishes, however, from the up-down symmetry of the polarization factor, $\alpha_{\mathrm{P}}(\theta) = \alpha_{\mathrm{P}}(\pi - \theta)$. Thus

$$\left(\frac{\partial \lambda_{\mathrm{TIRF}}}{\partial R_{\mathrm{ves}}}\right)_{R_{\mathrm{ves}}=0} = \frac{-\lambda_{\mathrm{TIRF}}(0)}{\delta_{\mathrm{TIRF}}}, \lambda_{\mathrm{TIRF}}(0) = \left(\frac{\mu_{\mathrm{Q}}}{2}\right) \int_0^{\pi} d\theta \sin\theta \, \alpha_{\mathrm{P}}(\theta) \, . \qquad \textbf{S18}$$

This shows that, at zero vesicle radius, λ_{TIRF} and its slope are determined by a simple moment of the polarization factor $\alpha_{\mathrm{P}}(\theta)$. To obtain $\lambda_{\mathrm{TIRF}}(0)$, in principle one could measure λ_{TIRF} versus vesicle radius (as described in this paper) and extrapolate to zero radius. In the main text we outlined an alternative procedure to obtain $\lambda^{\mathrm{o}}_{\mathrm{TIRF}} \equiv \lambda_{\mathrm{TIRF}}(0)$ which is based on the slope at the origin, and is preferable because our data is noisiest for small vesicles, whose small lipid release times are covered by fewest time frames in our intensity profiles. For small R_{ves} (we used data points with $R_{\mathrm{ves}} < 35$ nm) we fit our λ_{TIRF} versus R_{ves} data to a linear relation with the correct slope, as given by eq. **S18** (dashed red line, Fig. **6**D). Constraining this tangent to have intercept

$R_{\mathrm{ves}} = \delta_{\mathrm{TIRF}} = 68$ nm, the experimentally measured evanescent field penetration depth (see Materials and Methods), and extrapolating to zero vesicle size we could read off $\lambda^{\mathrm{o}}_{\mathrm{TIRF}} = 0.81 \pm 0.03$. For our experimental system, $\lambda^{\mathrm{o}}_{\mathrm{TIRF}}$ is essentially a pure polarization effect because self-quenching is expected to be negligible at the dilute lipid labeling densities we used (0.6-0.8 mole %, see Table S1).

Quantitative model of the effect of cholesterol on the fusion pore bending energy

A number of theoretical studies have analyzed the energetics of the membrane fusion pore (10, 11). Here we estimated the reduction by cholesterol of the bending energy of the highly bent fusion pore using a simple extension of a mathematical model developed in ref. (12). This is a strong effect because cholesterol has negative spontaneous curvature, and the fusion pore has a net negative curvature. The model quantifies the elastic properties of the lipid leaflets that constitute the pore. Our aim is to predict the influence of cholesterol on the free energy of pore formation, ΔF_{pore}, which is closely related to pore openness P_0 (see main text).

Consider two planar bilayers, whose neutral surfaces are separated by distance 2h (Fig. **S5**A). We assume each bilayer is symmetric and we will consider each of the physiologically motivated compositions that we treated in our experimental study (PC/PS/PE/PIP2, PC/PS/PE/PIP2/Ch, PC/PS/PE/PIP2/Ch+, Tables **S1, S2**.). What is the free energy to create a fusion pore, ΔF_{pore}? How is this free energy change affected by the addition of cholesterol? We assume the pore is torroidal in shape (10) with radius r_{p}. Hence each monolayer of the pore is also torroidal with dimensions adjusted by the monolayer thickness δ (Fig. **S5**A). Kozlov et al (12) calculated the elastic bending energy of such torroidal monolayers as

$$F_{\mathrm{monolayer}} = \pi\kappa \left\{ \frac{2\left(h + r_{\mathrm{p}}\right)^2}{h\sqrt{r_{\mathrm{p}}\left(r_{\mathrm{p}} + 2h\right)}} \operatorname{atan} \sqrt{\frac{r_{\mathrm{p}} + 2h}{r_{\mathrm{p}}}} + C_{\mathrm{o}}\left[2\pi\left(r_{\mathrm{p}} + h\right) - 8h\right] - 4 \right\} \qquad \textbf{S19}$$

where κ is the monolayer bending modulus and C_{o} is the monolayer spontaneous curvature. We applied this equation to the situation of two monolayers that constitute a fusion pore as follows. (1) Pore geometry required that the parameter h for membrane separation be increased

(decreased) by one-half of the monolayer thickness of 2 nm for the inner (outer) leaflets; we took an intermembrane headgroup separation of 7 nm so accordingly we used h=4.5 nm for the outer leaflets and h=6.5 nm for the inner leaflets. (2) Similarly the pore radius r_{p} was increased (decreased) by one-half of the monolayer thickness of 2 nm for the outer (inner) leaflets. (3) We calculated the spontaneous curvature C_{o} by taking the weighted average of all C_o values for the individual lipid species in the bilayer. For the inner and outer leaflets we used in the formula of Eq. S19 a spontaneous curvature equal to $-C_0$ and $+C_0$, respectively, reflecting the opposite orientations of the two leaflets. (4) We took the monolayer bending modulus to be $\kappa =$ 12 kT (13). (5) We summed the outer and inner monolayer energies to find the total energy of pore formation, $\Delta F_{\mathrm{pore}} = F^{\mathrm{outer}}_{\mathrm{monolayer}} + F^{\mathrm{inner}}_{\mathrm{monolayer}}$. For each membrane composition we allowed the pore radius to anneal, and we found that the pore radius corresponding to the lowest free energy of the fusion pore was independent of the spontaneous curvature of the individual leaflets.

To examine the mechanisms by which cholesterol may promote the open state of the fusion pore, we calculated the free energy advantage of adding cholesterol to the leaflets. In eq. **S19**, the different amounts of cholesterol had the effect of changing C_{o} (we assumed bending modulus κ was unaffected). To calculate the spontaneous curvature C_{o} for each level of cholesterol, we took the weighted average of the spontaneous curvature of each of the components. We took the spontaneous radius of curvatures of PC, PS, PE, and cholesterol to be -9.9, 14.4, -2.8, and -2.7 nm, respectively (13, 14). We find that the addition of moderate levels of cholesterol to physiological mimic compositions (45% and 10% cholesterol in SUV and SBL membranes, respectively, composition PC/PS/PE/PIP2/Ch) lowers the free energy of pore formation by ~8 kT, while with physiological cholesterol levels (46% in all membranes PC/PS/PE/PIP2/Ch+) the free energy of pore formation was lowered by ~43 kT (Fig. **S5**B). We note that the predicted free energies should be viewed as semi-quantitative because for simplicity of calculation it was assumed that the membranes are planar away from the pore, whereas in reality the vesicle membrane is curved.

Lipid compositions used in this study (details)

Symbol	PC (%)	DOPS (%)	SAPE (%)	PIP2 (%)	Chol (%)	Label (%)	PEG-PE	Label
$\boldsymbol{\alpha^{+}_{chol}}$	22.53	11.57	15.43	-	45.99	0.62	3.86	LR-PE
$\boldsymbol{\alpha_{chol}}$	23.75	12	15	-	45	0.8	3.45	LR-PE
	23.55	12	15	-	45	1	3.45	DiI
$\boldsymbol{\alpha}$	67.2	12	15	-	-	0.8	5	LR-PE
	67	12	15	-	-	1	5	DiI
	59.2	15	20	-	-	0.8	5	LR-PE
$\boldsymbol{\beta}$	79.2	15	-	-	-	0.8	5	LR-PE

Table S1-Lipid compositions for vesicle membranes. Symbols $\boldsymbol{\alpha^{+}_{chol}}$, $\boldsymbol{\alpha_{chol}}$, $\boldsymbol{\alpha}$, **and** $\boldsymbol{\beta}$ denote PC/PS/PE/PIP2/Ch+, PC/PS/PE/PIP2/Ch, PC/PS/PE/PIP2, and PC/PS, respectively. PC denotes 1-palmitoyl-2-oleoyl-*sn*-glycero-3-phosphocholine, POPC, except for composition $\boldsymbol{\beta}$ where it denotes 1,2-dioleoyl-*sn*-glycero-3-phosphocholine, DOPC; DOPS denotes 1,2-dioleoyl-*sn*-glycero-3-phospho-L-serine; SAPE denotes 1-stearoyl-2-arachidonoyl-*sn*-glycero-3-phosphoethanolamine; PIP2 denotes phosphatidylinositol 4,5-bisphosphate; LR denotes the fluorescent group lissamine rhodamine B.

Symbol	PC (%)	DOPS (%)	SAPE (%)	PIP2 (%)	Chol (%)	Label (%)	PEG-PE (%)
$\boldsymbol{\alpha^{+}_{chol}}$	18.91	11.57	15.43	3.86	45.99	0.38	3.86
$\boldsymbol{\alpha_{chol}}$	54.9	12	15	3	10	0.5	4.6
$\boldsymbol{\alpha}$	64.5	12	15	3	-	0.5	5
	54.5	15	20	5	-	0.5	5
$\boldsymbol{\beta}$	79.5	15	-	-	-	0.5	5

Table S2- Lipid compositions for SBL membranes. Symbols have same meaning as for Table S1. Label for SBL is NBD-PE, which denotes 1,2-dioleoyl-sn-glycero-3-phosphoethanolamine-N-(7-nitro-2-1,3-benzoxadiazol-4-yl).

Symbol	D_{lip} $(\mu m^2/s)$	Label
α^{+}_{chol}	0.45	LR-PE
α	1.17	LR-PE
	1.43	DiI
α_{chol}	1.49	LR-PE
	2.39	DiI
β	1.7	LR-PE

Table S3- Diffusion constants for each lipid membrane composition studied, and for each label used. Calculated from the measured mean square displacement curves for each composition (Fig. **S2B**).

Supporting References Cited

1. Karatekin, E., J. Di Giovanni, C. Iborra, J. Coleman, B. O'Shaughnessy, M. Seagar, and J. E. Rothman. 2010. A fast, single-vesicle fusion assay mimics physiological SNARE requirements. Proceedings of the National Academy of Sciences 107:3517-3521.
2. Smith, M. B., E. Karatekin, A. Gohlke, H. Mizuno, N. Watanabe, and D. Vavylonis. 2011. Interactive, Computer-Assisted Tracking of Speckle Trajectories in Fluorescence Microscopy: Application to Actin Polymerization and Membrane Fusion. Biophysical journal 101:1794-1804.
3. Klyachko, V. A., and M. B. Jackson. 2002. Capacitance steps and fusion pores of small and large-dense-core vesicles in nerve terminals. Nature 418:89-92.
4. Breckenridge, L., and W. Almers. 1987. Final steps in exocytosis observed in a cell with giant secretory granules. Proceedings of the National Academy of Sciences 84:1945.
5. Monck, J. R., and J. M. Fernandez. 1992. The exocytotic fusion pore. The Journal of Cell Biology 119:1395.
6. He, L., X. S. Wu, R. Mohan, and L. G. Wu. 2006. Two modes of fusion pore opening revealed by cell-attached recordings at a synapse. Nature 444:102-105.
7. Wagner, M. L., and L. K. Tamm. 2001. Reconstituted syntaxin1a/SNAP25 interacts with negatively charged lipids as measured by lateral diffusion in planar supported bilayers. Biophysical journal 81:266-275.
8. Shi, L., Q. T. Shen, A. Kiel, J. Wang, H. W. Wang, T. J. Melia, J. E. Rothman, and F. Pincet. 2012. SNARE proteins: one to fuse and three to keep the nascent fusion pore open. Science Signalling 335:1355.
9. Axelrod, D. 1989. Total internal reflection fluorescence microscopy. Method Cell Biol. 30:245-270.
10. Chizmadzhev, Y. A., F. Cohen, A. Shcherbakov, and J. Zimmerberg. 1995. Membrane mechanics can account for fusion pore dilation in stages. Biophysical journal 69:2489-2500.
11. Jackson, M. B. 2009. Minimum membrane bending energies of fusion pores. J. Membr. Biol. 231:101-115.
12. Kozlov, M. M., S. L. Leikin, L. V. Chernomordik, V. S. Markin, and Y. A. Chizmadzhev. 1989. Stalk mechanism of vesicle fusion - intermixing of aqueous contents. Eur. Biophys. J. Biophys. Lett. 17:121-129.
13. Chen, Z., and R. Rand. 1997. The influence of cholesterol on phospholipid membrane curvature and bending elasticity. Biophysical journal 73:267-276.
14. Fuller, N., C. R. Benatti, and R. Peter Rand. 2003. Curvature and bending constants for phosphatidylserine-containing membranes. Biophys. J. 85:1667-1674.

Supplementary Figures

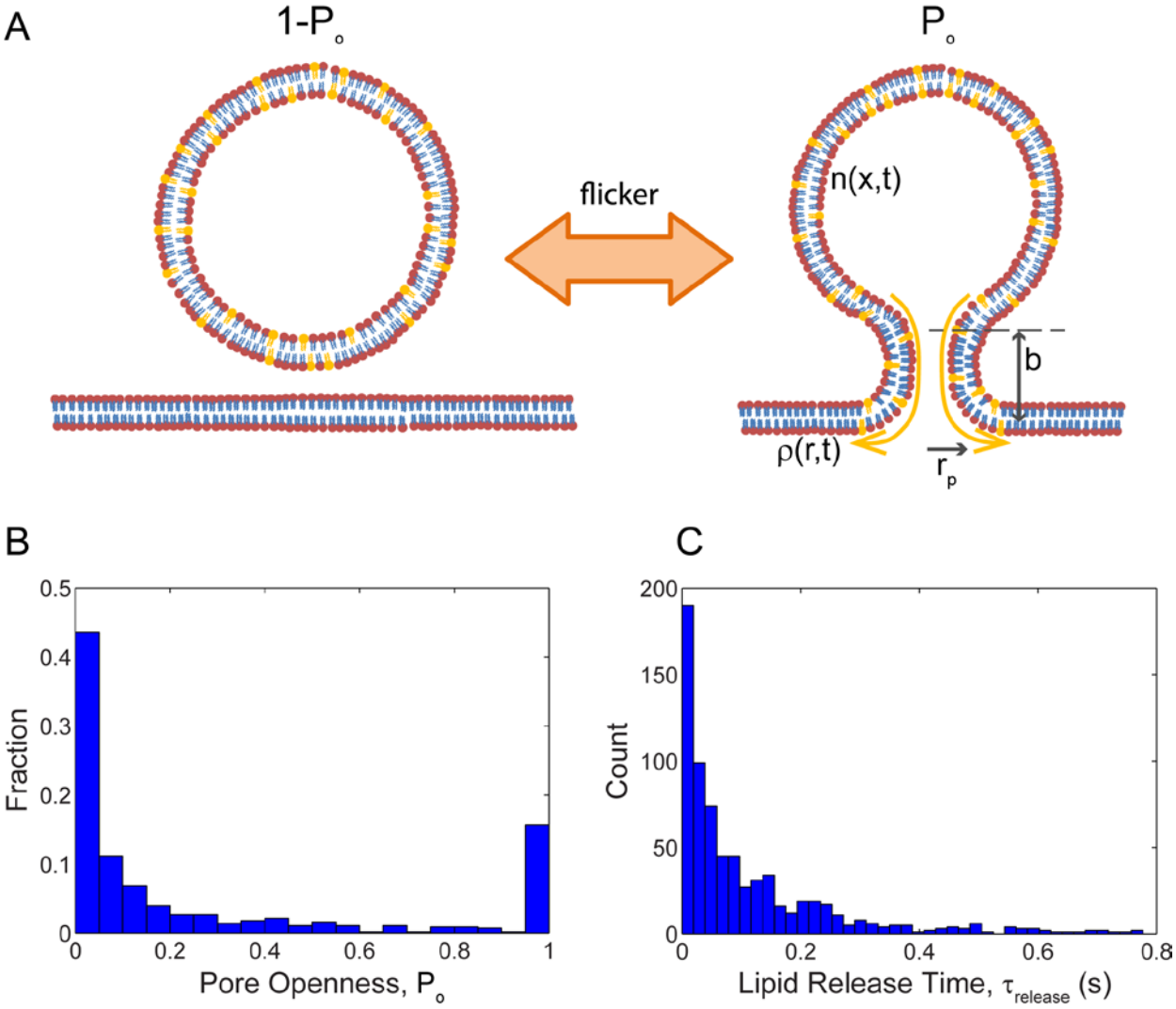

Figure S1- (A) Model of lipid release from a vesicle through a flickering fusion pore. Schematic of model. The pore is centered at $x = 0$ in the vesicle and $r = 0$ in the SBL. The density of labelled lipids in the vesicle is $n(x,t)$ and in the SBL is $\rho(r,t)$. Here, we model the pore as a cylinder of length $b = 15$ nm and radius $r_p = 3$ nm. The pore radius is measured from the center of the pore to the centerline of the bilayer. During open periods of the pore, lipids can diffuse through the membranes of the neck of the pore into the SBL membranes; the net flux is proportional to the density difference across the pore multiplied by the fraction of the time the pore is open, P_o (eqs. S1 and S2). (B) Measured overall distribution of P_o values, for all compositions. Mean openness for flickering pores is 0.14 ± 0.01 and the fraction of pores that are permanently open is 15%. Bin size 0.05. (C) Measured distribution of lipid release times across all compositions. Bin size is 0.02 s.

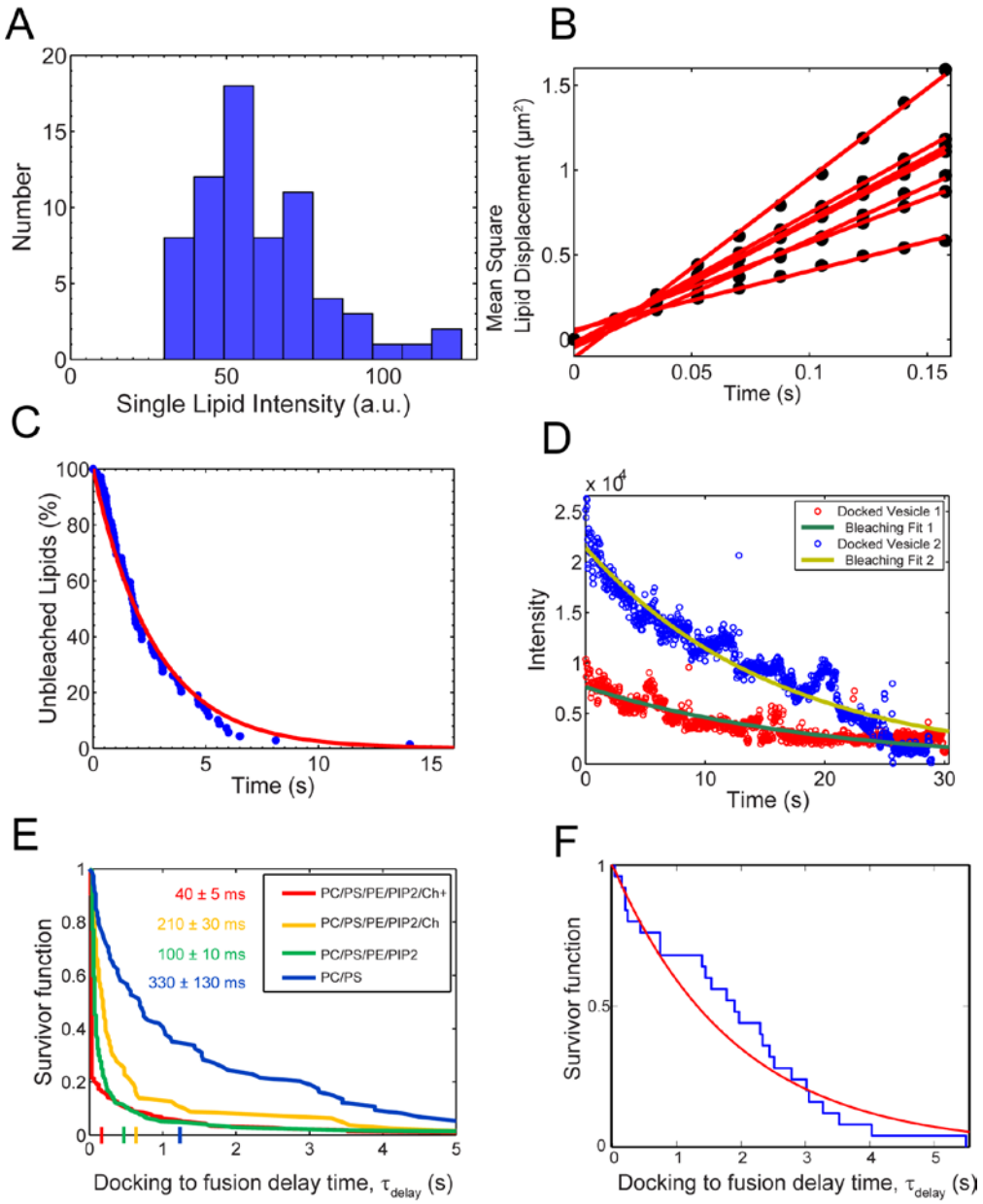

Figure S2- Single lipid properties needed for fusion event analysis, and measured docking-to-fusion delay time distributions. (A-C) Single lipid resolution enables accurate measurement of diffusivity, bleaching time and single lipid emission. Plots shown for PC/PS membrane composition. (A) Distribution of measured single lipid intensities, I_{lip}, in a typical movie. (B) Mean square displacement versus time for seven lipid trajectories. (C) Digital measurement of bleaching time τ_{bleach}. Labeled lipids in the SBL suddenly ceased fluorescing, indicating that these fluorescing spots were individual lipids. The survivor fraction is shown for a sample movie, fit to an exponential $\exp -t/\tau_{\mathrm{bleach}}$ (red curve). (D) Bleaching of lipids in vesicles is much slower than for lipids in the SBL. Emission intensity versus time for two representative unfused vesicles. Each is shown with a best fit curve to a decaying exponential $I(t) = e^{-t/\tau_{\mathrm{bleach}}^{\mathrm{ves}}}$ where $\tau_{\mathrm{bleach}}^{\mathrm{ves}}$ is the bleaching time in the vesicle. Both events are for PC/PS/PE/PIP2/Ch+ membrane composition. The bleaching time of the Docked Vesicle 1 (data: red points, best fit exponential:

green curve) is 19.9 s. The bleaching time for Docked Vesicle 2 (data: blue points, best fit exponential: gold curve) is 16.0 s. Both values are much greater than $3s \lesssim \tau_{\mathrm{bleach}} \lesssim 5s$, the bleaching time in the SBL. (E) Docking-to-fusion delay time distributions: measured survivor functions for all compositions. Mean delay times $\overline{\tau}_{\mathrm{delay}}$ for each composition are shown, along with 95% confidence interval. Colored ticks on the x-axis indicate the cutoff times used to separate the SNARE-mediated and non-specific fusion events. The cutoff times were obtained by fitting double exponentials to the survivor functions. (F) Docking-to-fusion delay time distributions for fusions between protein-free SBLs and v-SNARE containing SUVs, for lipid composition PC/PS/PE/PIP2/Ch that contains 45% (10%) cholesterol in the SUV (SBL) (see Tables **S1, S2**). Measured survivor function (blue curve) and best fit exponential (red curve) with delay time $\overline{\tau}_{\mathrm{pf}} = 1.9$ s are plotted. There is no statistically significant difference between this distribution and the long tail of the slow component of the delay time distribution for PC/PS/PE/PIP2/Ch fusion events between v-SUVs and t-SBLs ($p>0.05$), part (E).

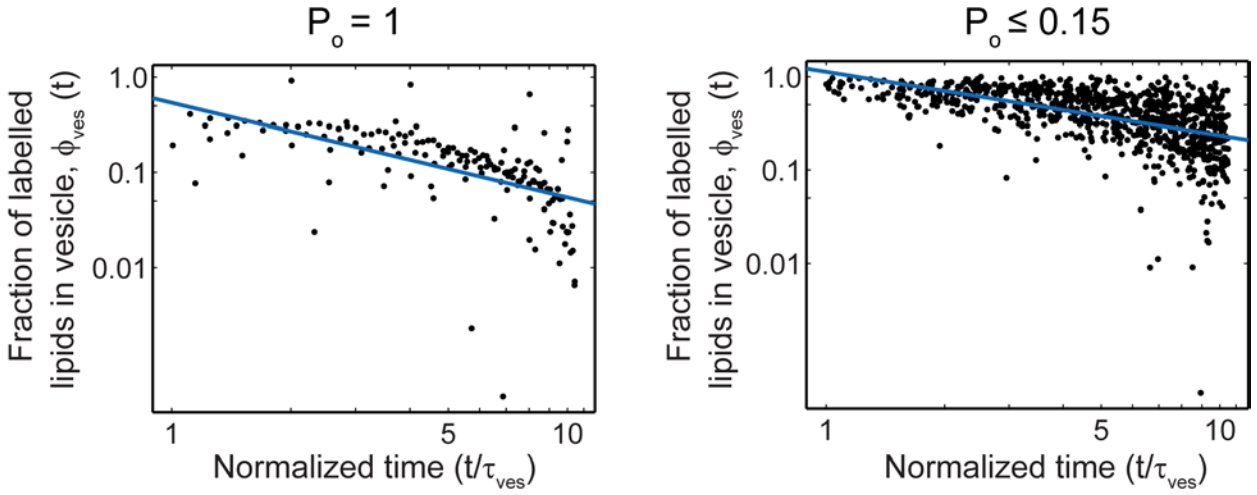

Figure S3- Vesicle-to-SBL lipid release kinetics through permanently open pores have power law dependence on time. Our model predicts that the number of lipids remaining in the vesicle decays as $\phi_{\mathrm{ves}}(\mathrm{t}) \sim \tau_{\mathrm{ves}}/t$ for a fully open fusion pore where τ_{ves} is the diffusion time on the scale of the vesicle and depends on vesicle size (see main text). The pooled $\phi_{\mathrm{ves}}(t)$ data that we measured for all fully open fusion pores ($P_{\mathrm{o}} = 1$, left panel) collapsed onto a single power law relation when plotted against time scaled with τ_{ves}. The best fit power law (blue line) was $t^{-\alpha}$ with $\alpha = -0.99 \pm 0.22$, very close to the model prediction. The same procedure applied to flickering pores with relatively small openness ($P_{\mathrm{o}} \leq 0.15$, right panel) produced a best fit power law exponent $\alpha = -0.68 \pm 0.09$.

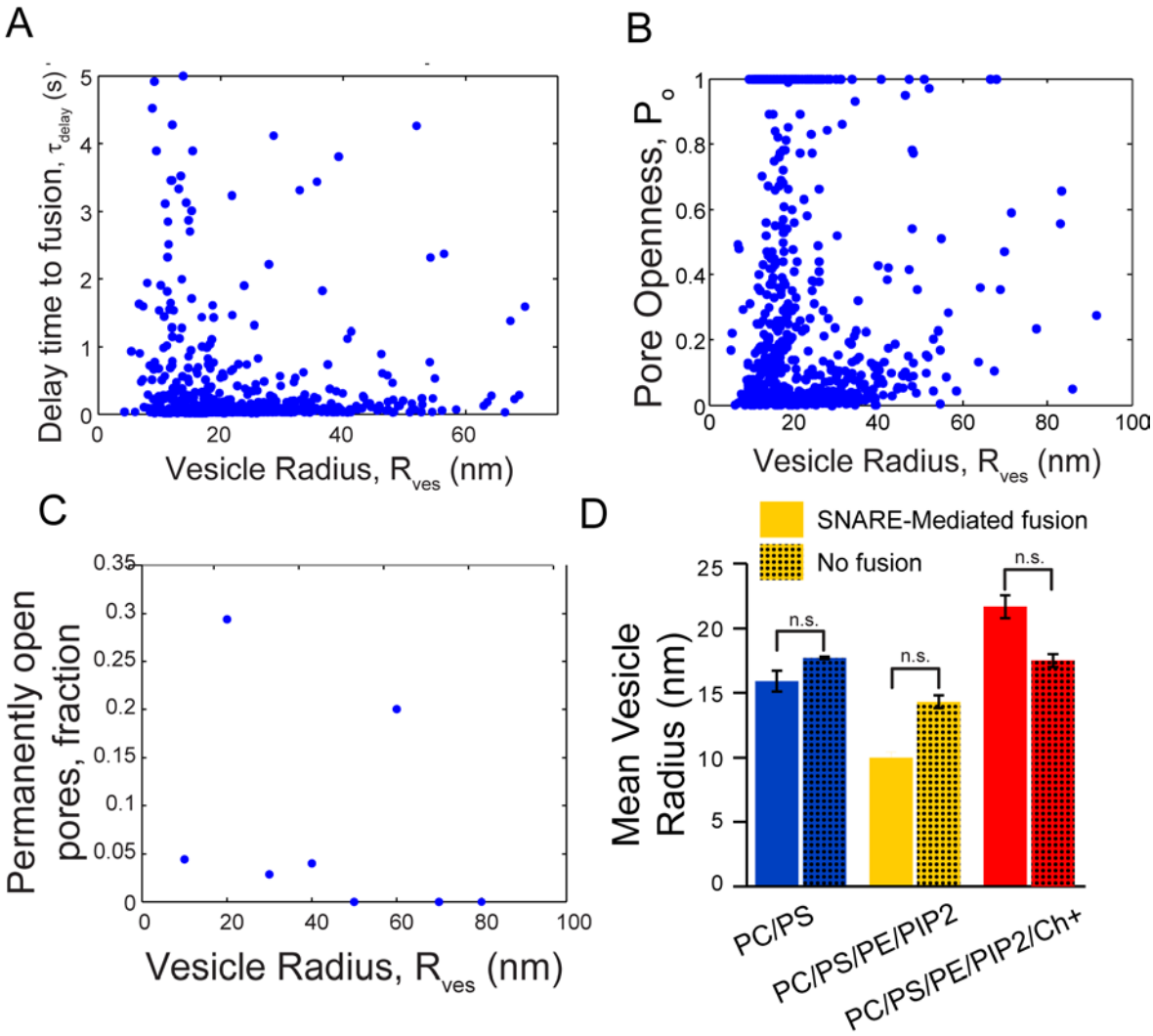

Figure S4- Statistics of fusion reveal no dependence on vesicle size. (A) Docking-to-fusion delay times versus vesicle size showed no correlations ($c_{\mathrm{corr}} = -0.04$, n=772, SNARE-mediated and non-specific events). Data shown represents all fusion events measured in this study for which both SBL and SUV membranes contained SNARES, for all compositions (Tables **S1,S2**). (B) Pore openness is not correlated with vesicle size, ($c_{\mathrm{corr}} = 0.05$, n=555 specific fusion events). Data shown represents all SNARE-mediated fusion events measured in this study (fast component of delay time distribution) for all compositions. (C) Fraction of pores that are permanently open is not correlated with vesicle size (c_{corr} = -0.04). Bin size 10nm. Same fusion events as for (B). (D) Mean size of vesicles that undergo SNARE-mediated fusion (solid bars) is statistically indistinguishable from mean size of docked vesicles that do not fuse during the bleaching time (dotted bars), $P > 0.05$. The comparison is shown for three lipid membrane compositions.

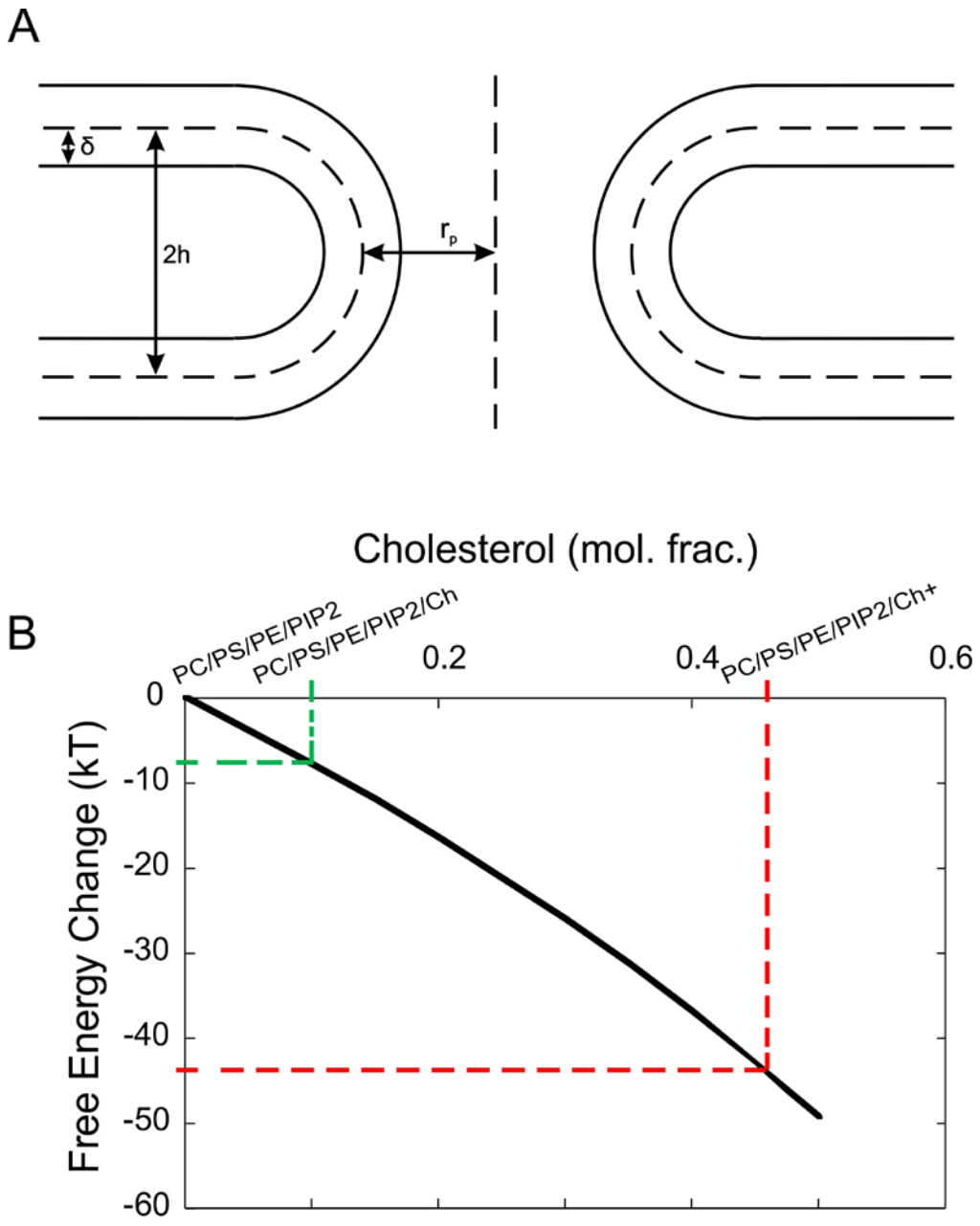

Figure S5- Cholesterol lowers the bending energy of fusion pores: calculation of pore bending energy using an elastic model of the fusion pore. (A) Schematic of a fusion pore, side view. The membranes have asymptotic separation 2h and the pore radius is r_p. Each leaflet has thickness δ. (B) Free energies were calculated for the biologically motivated family of lipid compositions (Tables S1, S2) using eq. **S20**. The change in free energy of pore formation relative to zero cholesterol (PC/PS/PE/PIP2) is plotted versus cholesterol content. Values for the two cholesterol-rich compositions studied (PC/PS/PE/PIP2/Ch, PC/PS/PE/PIP2/Ch+) are indicated. High cholesterol levels produce enormous free energy decreases, indicating a powerful stabilizing effect on the open state of the pore.

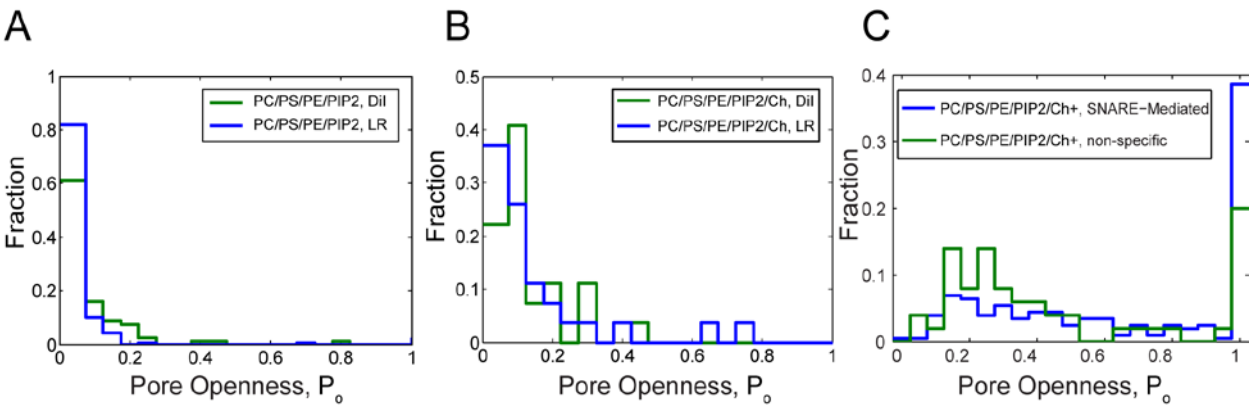

Figure S6- (A, B). Measured distributions of pore openness were not significantly different ($p>0.05$, student's t-test) for two distinct fluorescent lipid labels, lissamine-rhodamine-tagged PE (LR-PE) and the lipophilic dye DiI. This was true for both lipid compositions PC/PS/PE/PIP2 and PC/PS/PE/PIP2/Ch. These results are consistent with LR-PE diffusion not being anomalously suppressed in the fusion pore and the validity of the P_o values inferred from release kinetics of LR-PE through fusion pores. (C) Distributions of fusion pore openness for SNARE-mediated and non-specific fusion events between membranes having high cholesterol content (lipid composition PC/PS/PE/PIP2/Ch+). The fraction of pores that were fully open was ~2-fold higher when SNAREs mediated the pores.

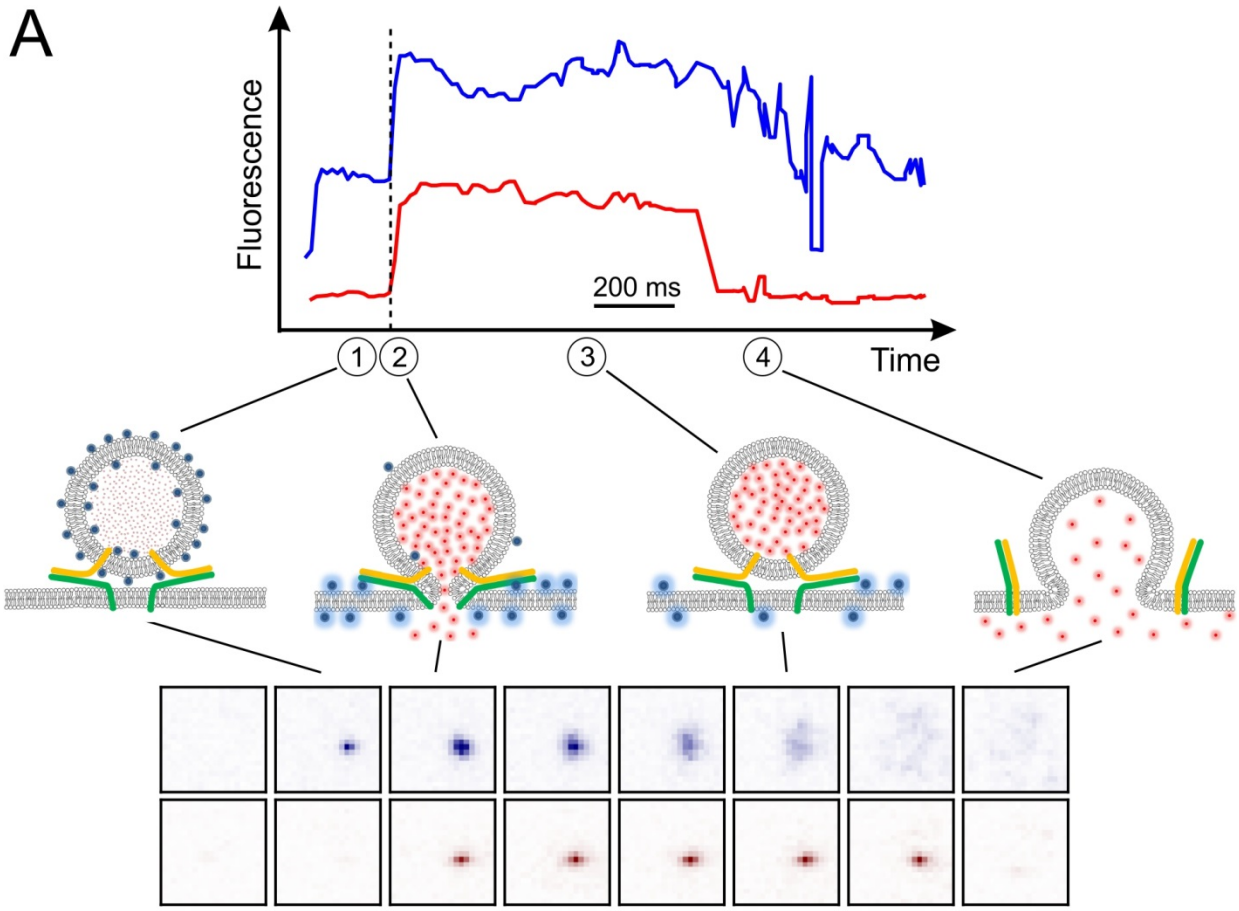
A
Fluorescence
200 ms
Time
1
2
3
4

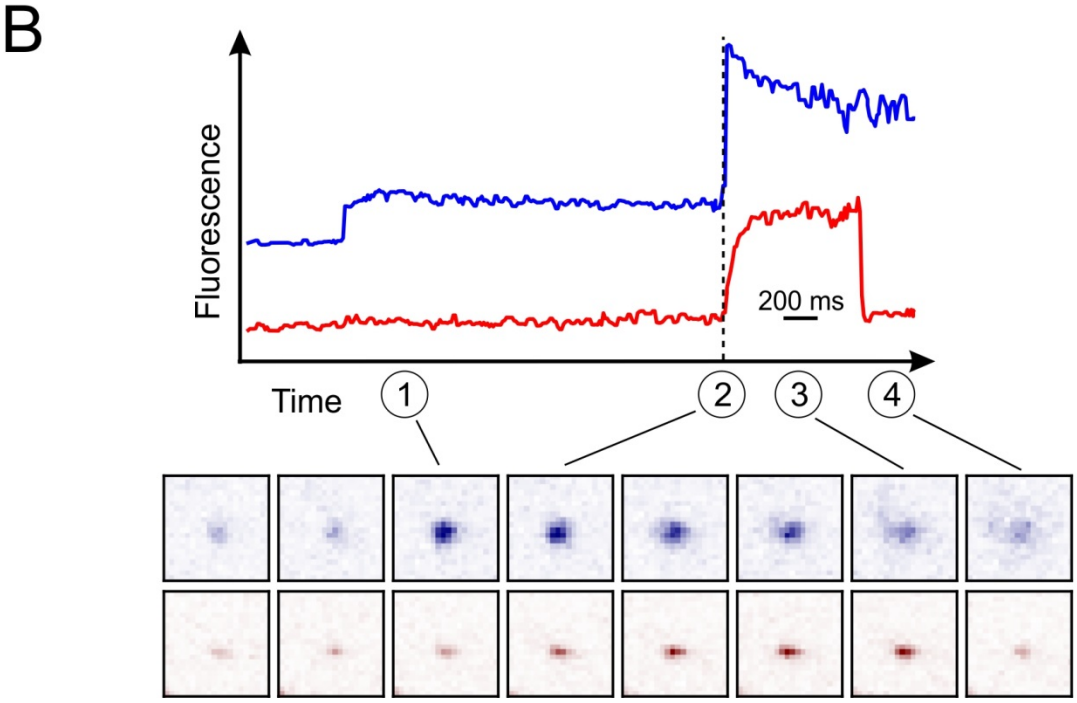
B
Fluorescence
200 ms
Time
1
2
3
4

Figure S7- Additional examples of simultaneous contents and lipid release during v-SUV/t-SBL fusion, measured with TIRFM (cf. Fig 3). (A) vSUVs with 45 mole % cholesterol, (B) cholesterol-free vSUVs contained 1 mole % DiD lipid dye and encapsulated 10 mM soluble contents marker SRB. DiD and SRB were simultaneously excited using 638 nm and 561 nm laser lines, respectively. The emission was split to observe DiD (top trace, blue) and SRB (red trace) fluorescence signals simultaneously projected onto an EMCCD detector. Total intensities from a region 20 pixels by 20 pixels (5.3 μm x 5.3 μm) are plotted (18.3 ms resolution) for both the lipid (upper trace, blue) and contents (lower trace, red) signals for representative events. Snapshots from the lipid (blue) and contents (red) signals are shown in inverted false colors. When docking was clearly visible in the lipid channel, the contents channel was still dim, because SRB was encapsulated at self-quenching concentrations (#1). In the same frame in which the lipid signals begin to increase, announcing lipid mixing, the contents signals also increase (dashed vertical line), due to dilution and dequenching of encapsulated SRB as molecules escape through the pore. Once lipid transfer is complete (shortly after the maximum in the blue trace), the intensity in the lipid channel decreases due to photobleaching (#3), as in Fig. 2. The SRB signal was abruptly lost seconds after the initial dequenching (#4) in ~20% of events. .